Electronic Supplementary Material (ESI) for RSC Advances.

Supporting information

Experimental and DFT studies of Sulfadiazine 'piano-stool' Ru(II) and Rh(III) complexes

Ahmed M Mansour, *[a] and Krzysztof Radacki [b]

[a] Department of Chemistry, Faculty of Science, Cairo University,

Gamma Street, Giza, Cairo 12613, Egypt

[b] Institut für Anorganische Chemie, Julius-Maximilians-Universität Würzburg,

Am Hubland, D-97074 Würzburg, Germany

* mansour@sci.cu.edu.eg;

ahmed.mansour@uni-wuerzburg.de

* Corresponding author

Figure S1	AT IR spectra of sulfadiazine complexes, a) **1**, and b) **2**.
Figure S2	NMR analysis of **1** in CD_3SOCD_3, a) ^1H, b) ^{13}C, c) {^1H, ^1H} COS90, d) {^{13}C, ^1H} HSQC and e) ^{13}C DEPT spectra.
Figure S3	NMR analysis of **2** in CD_3SOCD_3, a) ^1H, b) ^{13}C, c) {^1H, ^1H} COS90, d) {^{13}C, ^1H} HSQC, e) ^{13}C DEPT and f) [^1H–^{15}N] HMBC spectra.
Figure S4	NMR analysis of Na$\mathbf{L^{SZ}}$ in CD_3SOCD_3, a) ^1H, b) ^{13}C, c) contour [^1H–^{15}N] HMBC and d) oblique [^1H–^{15}N] HMBC spectra.
Figure S5	Crystal packing of **2** showing the intermolecular H-bond of the type NH_2…OSO_2.
Table S1	Selected bond lengths and angles of organometal compounds **1** and **2.**
Table S2	Computed excitation energies (eV), electronic transition configurations and oscillator strengths (*f*) of the studied complexes (selected, ($f > 0.002$) calculated at CAM-B3LYP/ LANL2DZ level of theory.
Figure S6	Calculated electronic spectra of the complexes studied here using CAM-B3LYP/ LANL2DZ method; a) full spectrum and b) 250–600 nm.
	Biological part

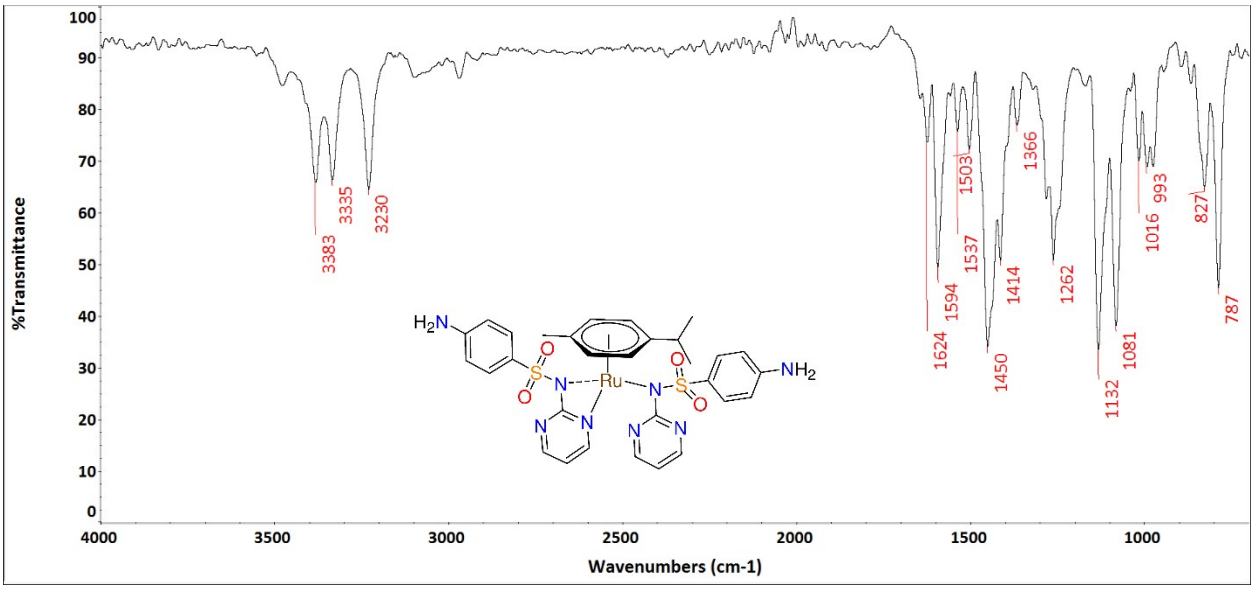

a)

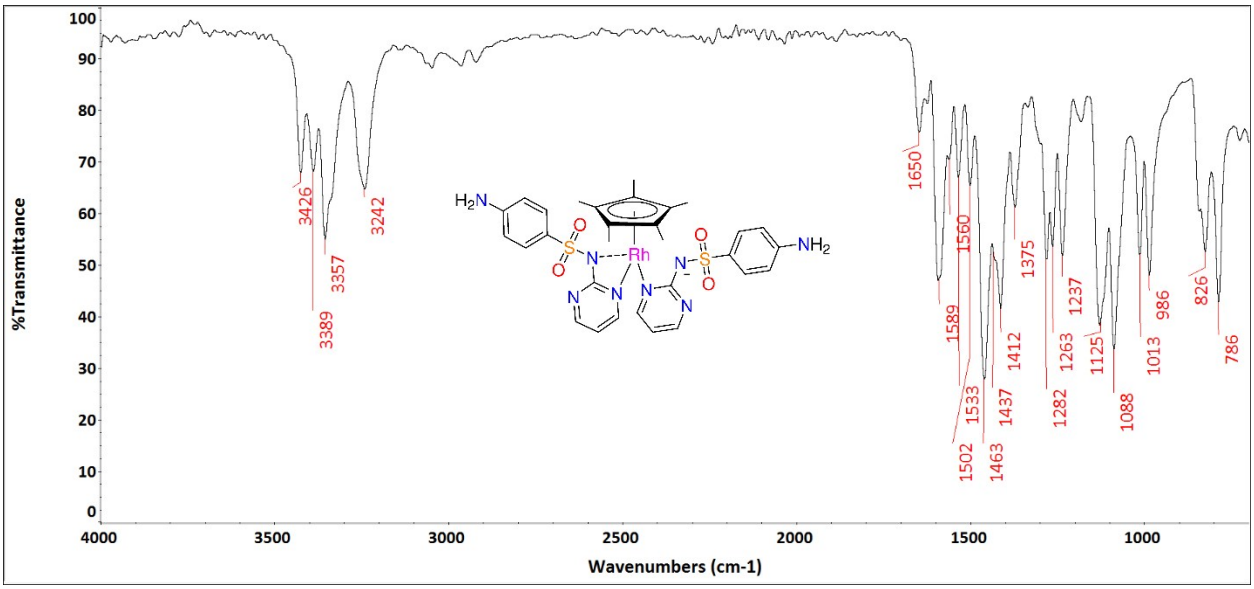

b)

Figure S1 AT IR spectra of Sulfadiazine complexes a) **1**, and b) **2**.

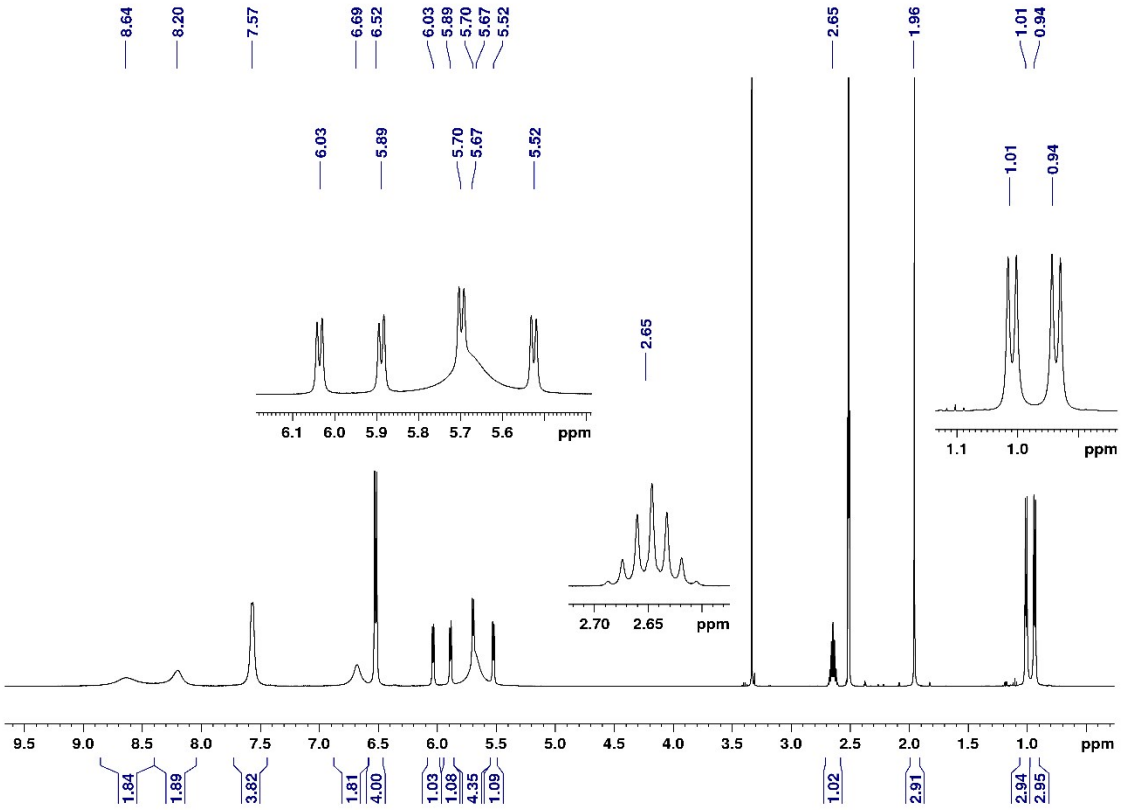
8.64
8.20
7.57
6.69
6.52
6.03
5.89
5.70
5.67
5.52
2.65
1.96
1.01
0.94
ppm
1.84
1.89
3.82
1.81
4.00
1.03
1.08
4.35
1.09
1.02
2.91
2.94
2.95

a)

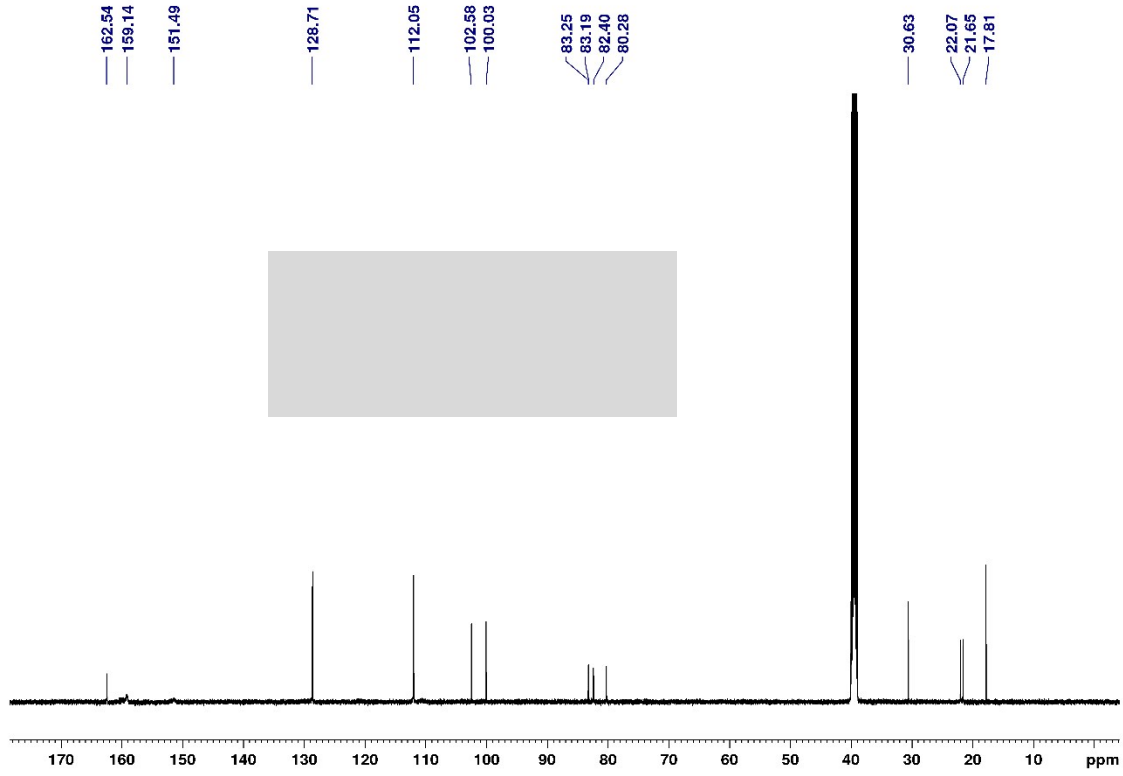
162.54
159.14
151.49
128.71
112.05
102.58
100.03
83.25
83.19
82.40
80.28
30.63
22.07
21.65
17.81
ppm

b)

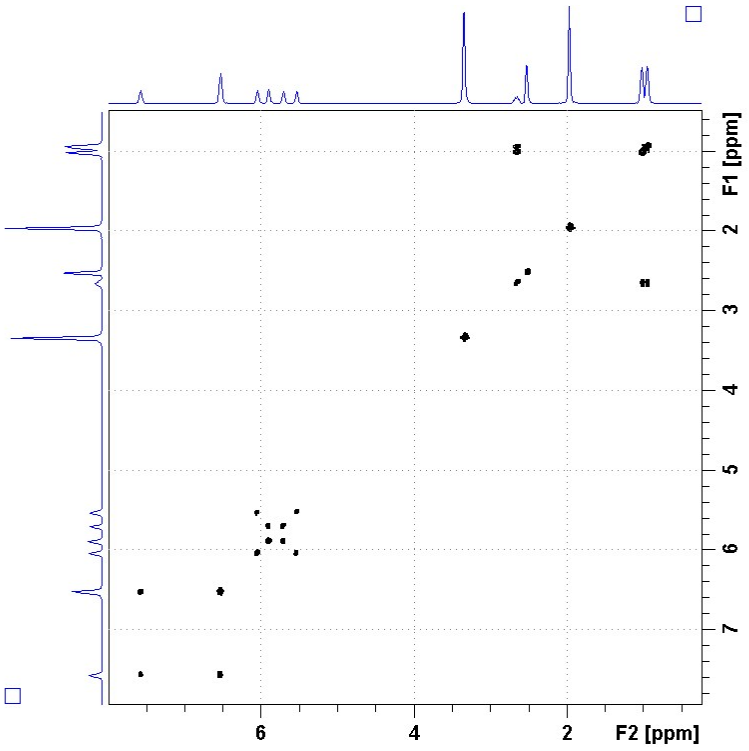

c)

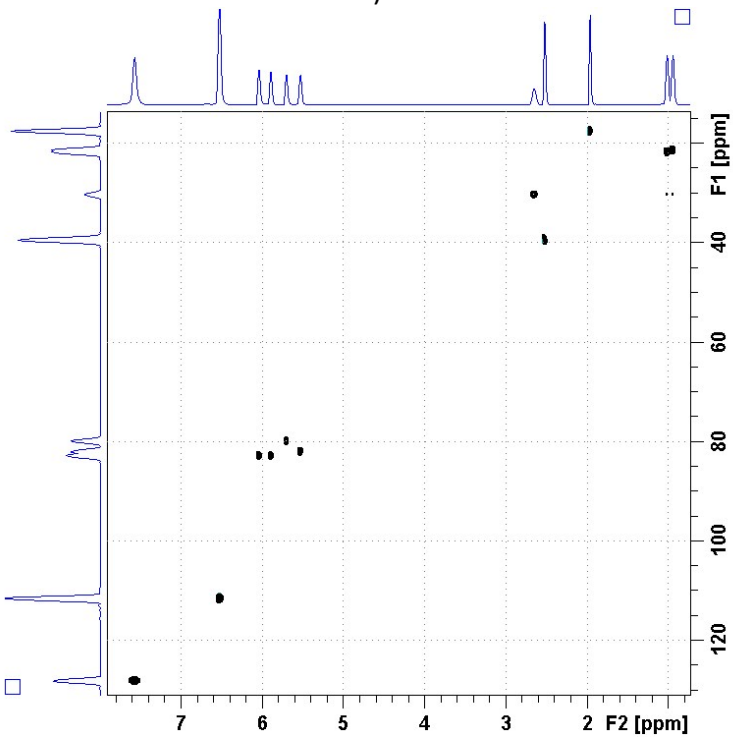

d)

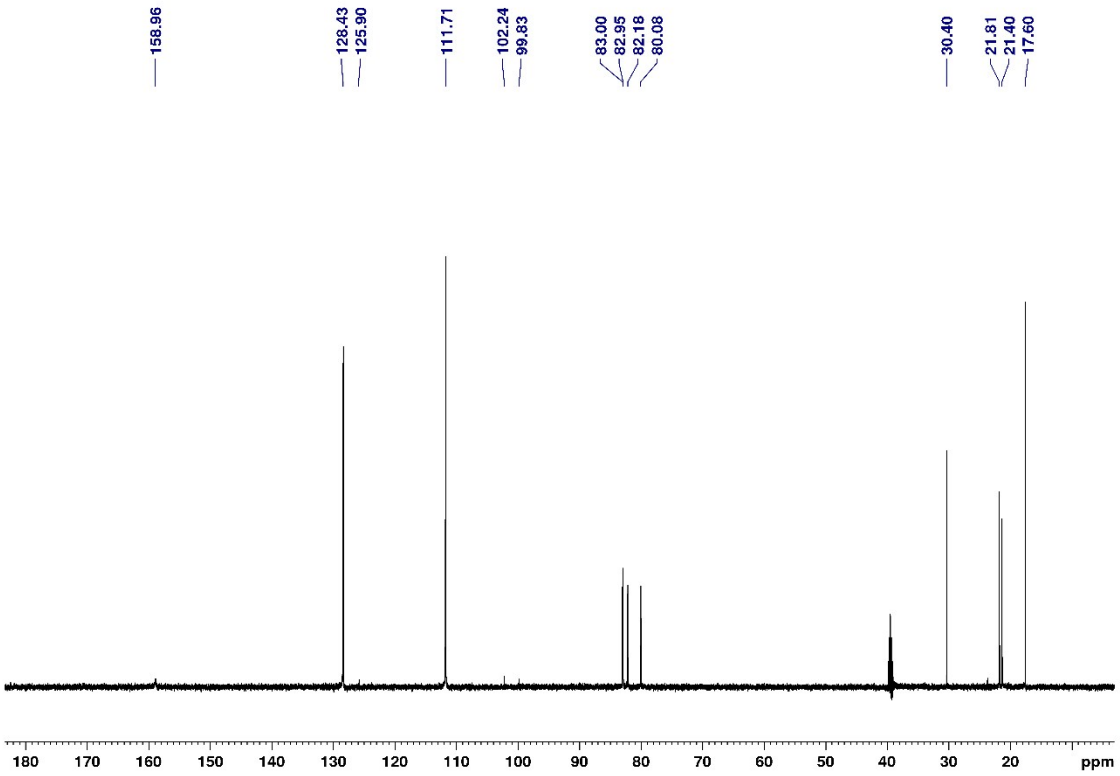

e)

Figure S2 NMR analysis of **1** in CD_3SOCD_3, a) ^1H, b) ^{13}C, c) {^1H, ^1H} COS90, d) {^{13}C, ^1H} HSQC and e) ^{13}C DEPT spectra.

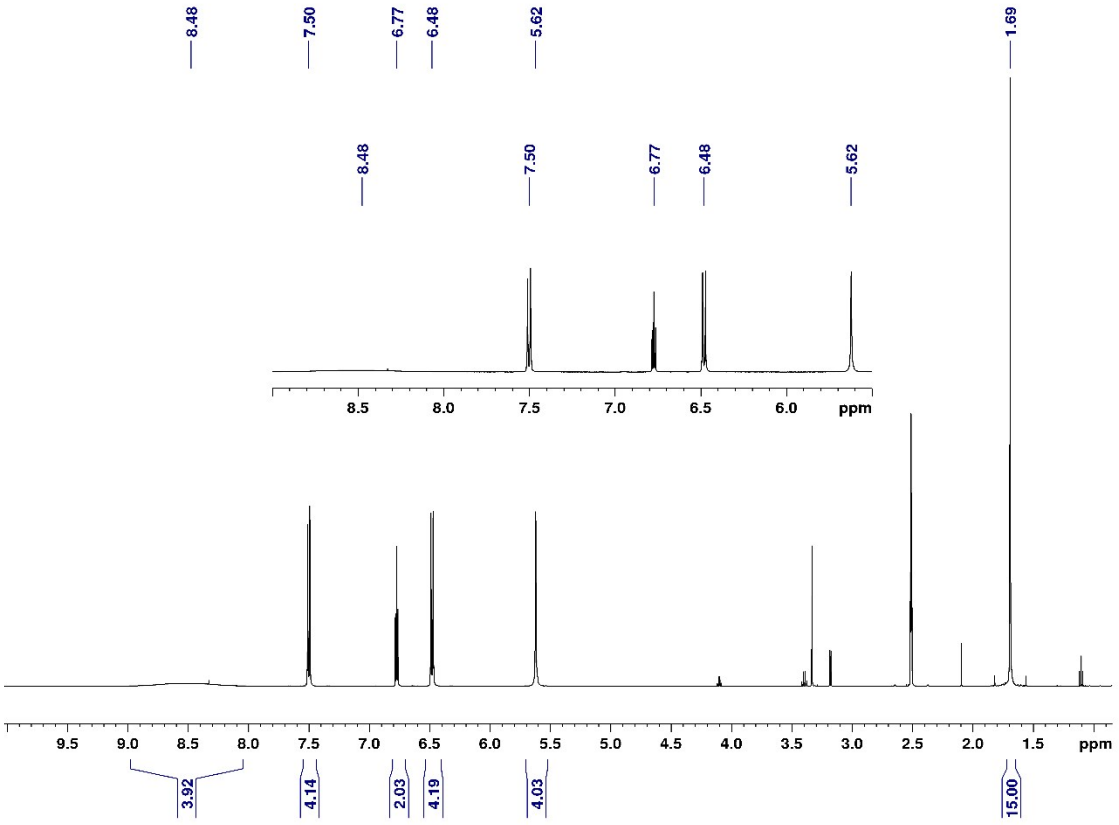
8.48
7.50
6.77
6.48
5.62
1.69
8.5
8.0
7.5
7.0
6.5
6.0
ppm
9.5
9.0
8.5
8.0
7.5
7.0
6.5
6.0
5.5
5.0
4.5
4.0
3.5
3.0
2.5
2.0
1.5
ppm
3.92
4.14
2.03
4.19
4.03
15.00

a)

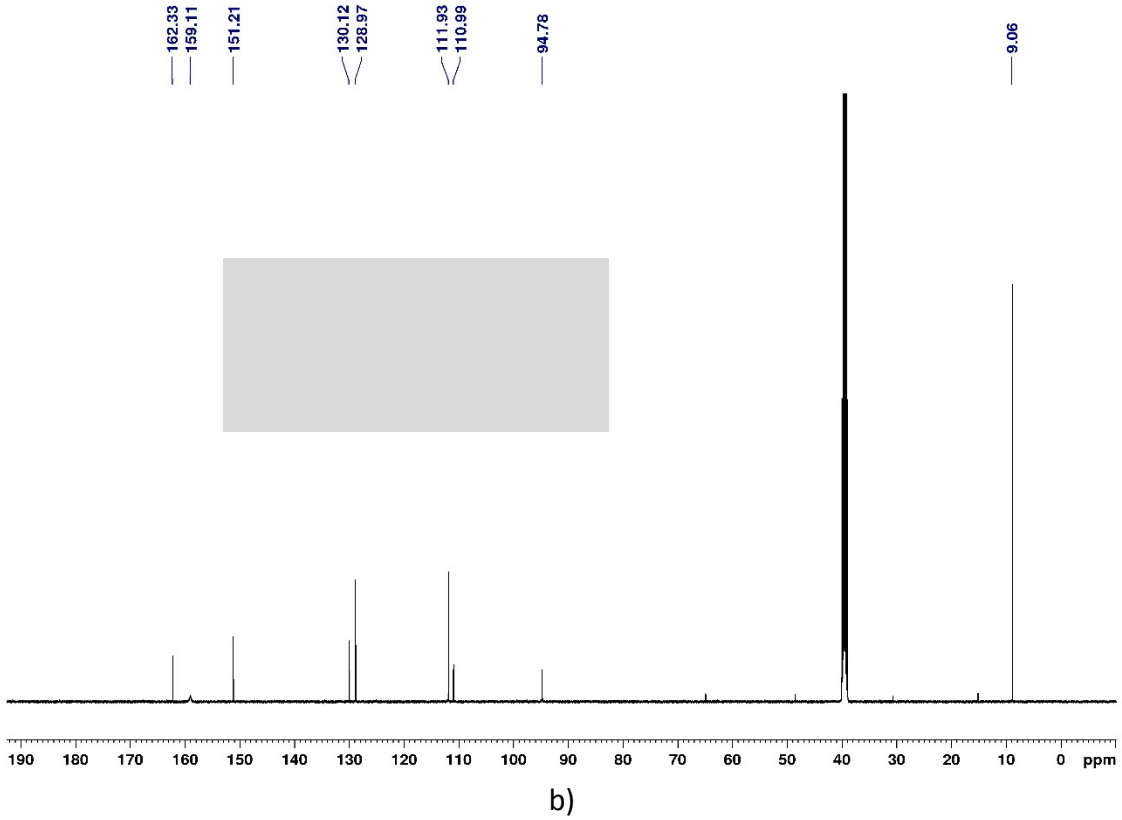
162.33
159.11
151.21
130.12
128.97
111.93
110.99
94.78
9.06
190
180
170
160
150
140
130
120
110
100
90
80
70
60
50
40
30
20
10
0
ppm

b)

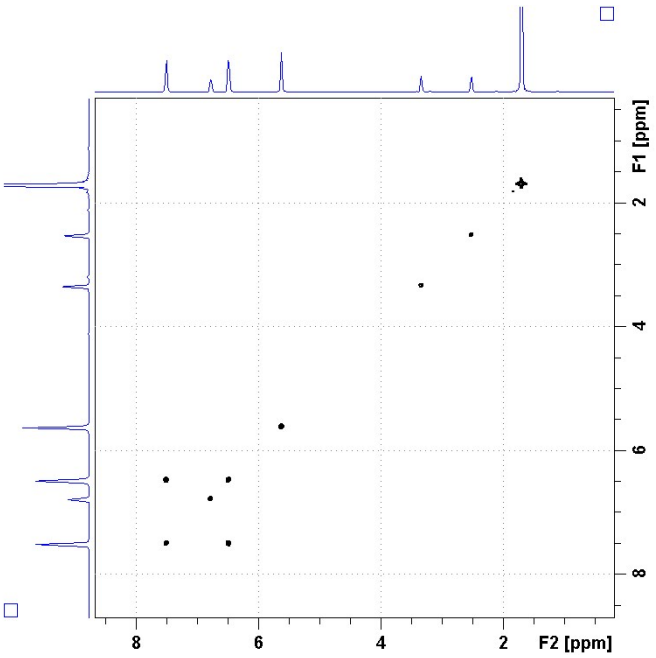

c)

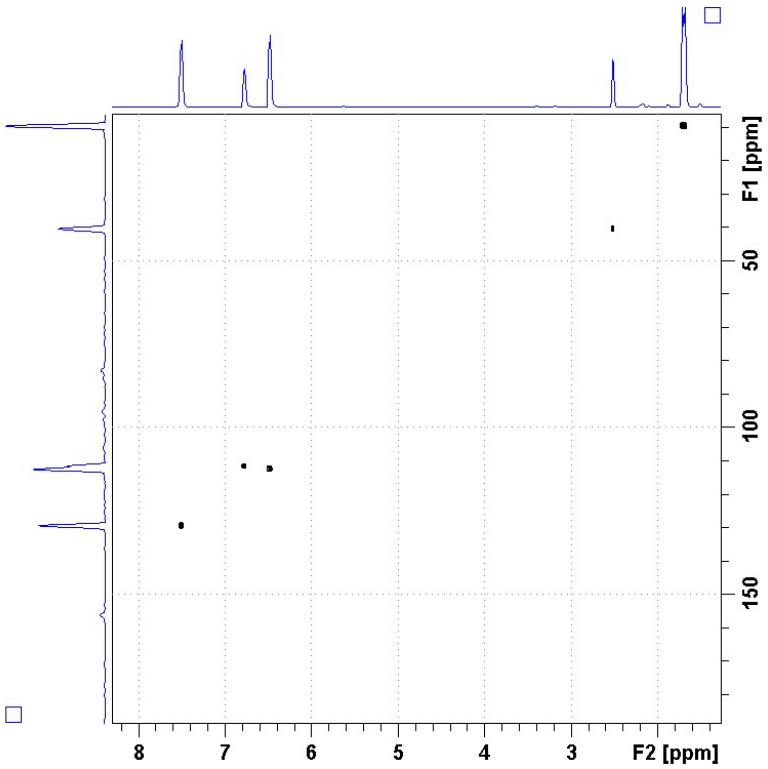

d)

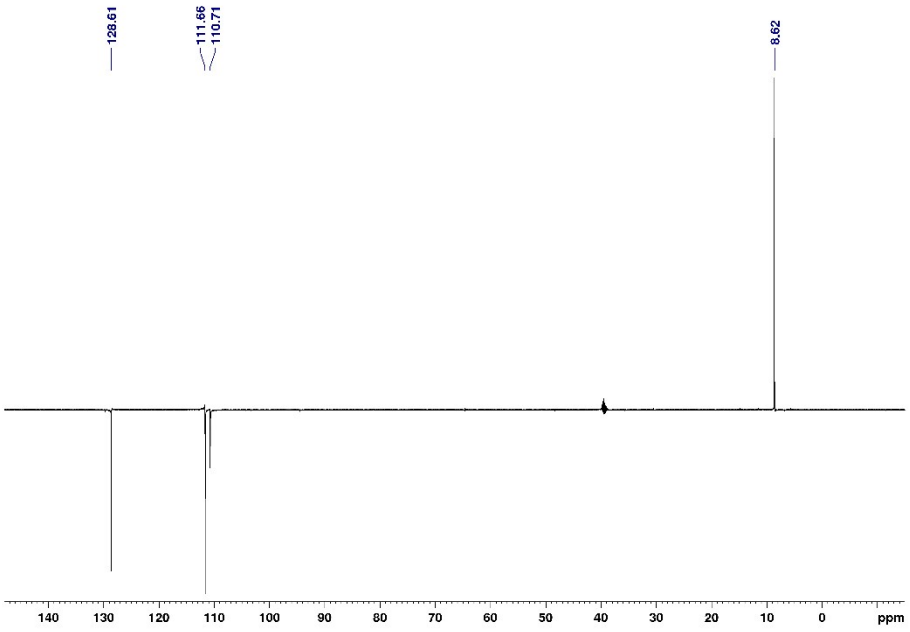

e)

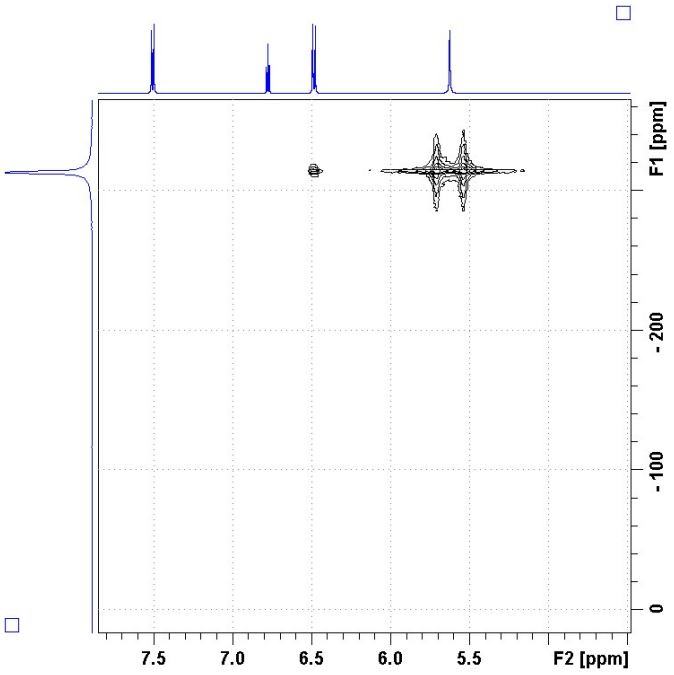

f)

Figure S3 NMR analysis of **2** in CD_3SOCD_3, a) ^{1}H, b) ^{13}C, c) {^{1}H, ^{1}H} COS90, d) {^{13}C, ^{1}H} HSQC, e) ^{13}C DEPT and f) [^{1}H–^{15}N] HMBC spectra.

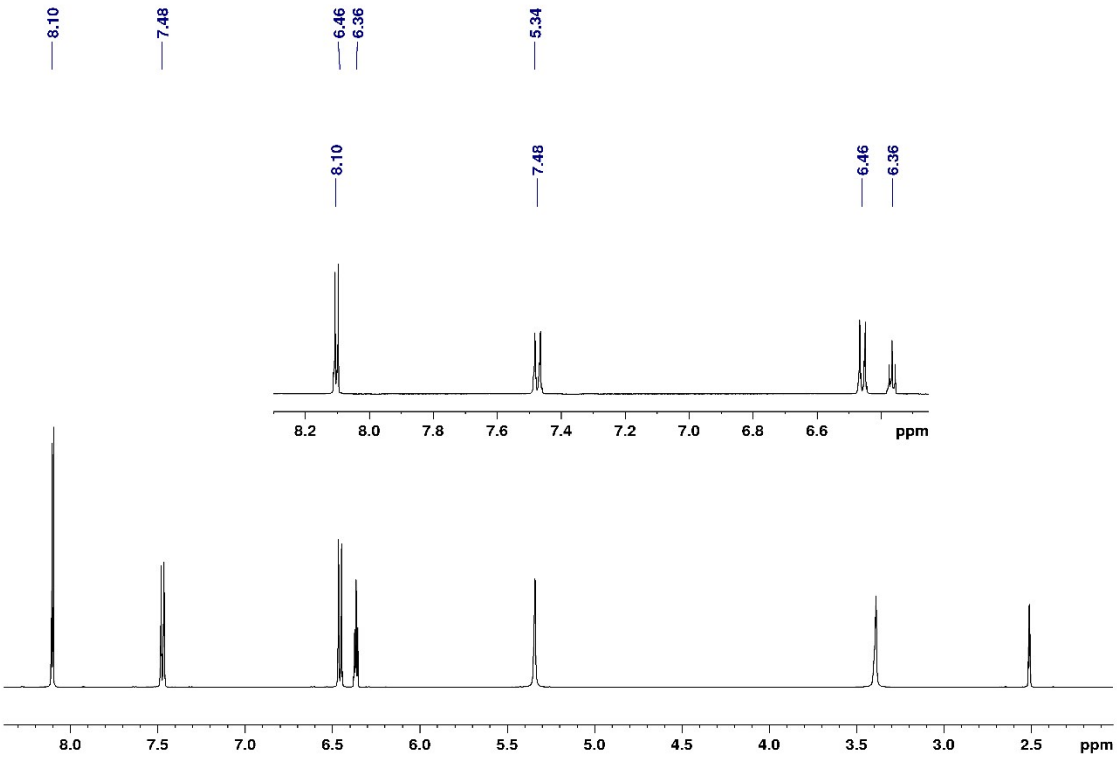
8.10
7.48
6.46
6.36
5.34
8.10
7.48
6.46
6.36
8.2
8.0
7.8
7.6
7.4
7.2
7.0
6.8
6.6
ppm
8.0
7.5
7.0
6.5
6.0
5.5
5.0
4.5
4.0
3.5
3.0
2.5
ppm

a)

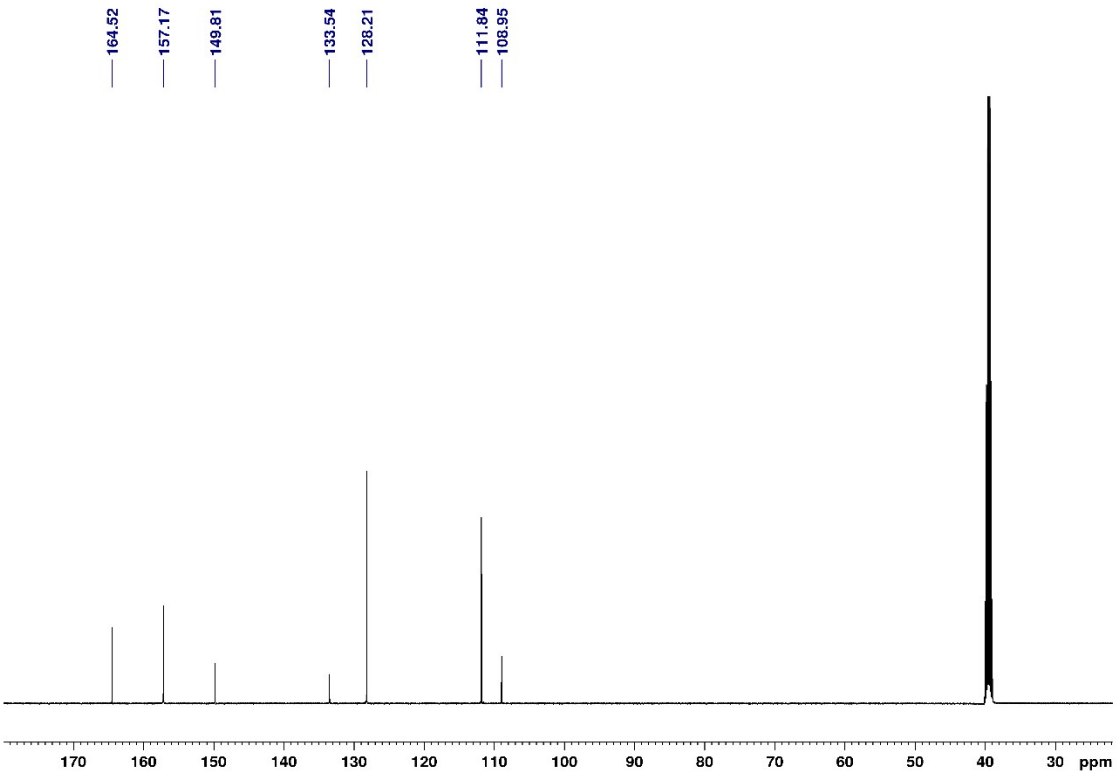
164.52
157.17
149.81
133.54
128.21
111.84
108.95
170
160
150
140
130
120
110
100
90
80
70
60
50
40
30
ppm

b)

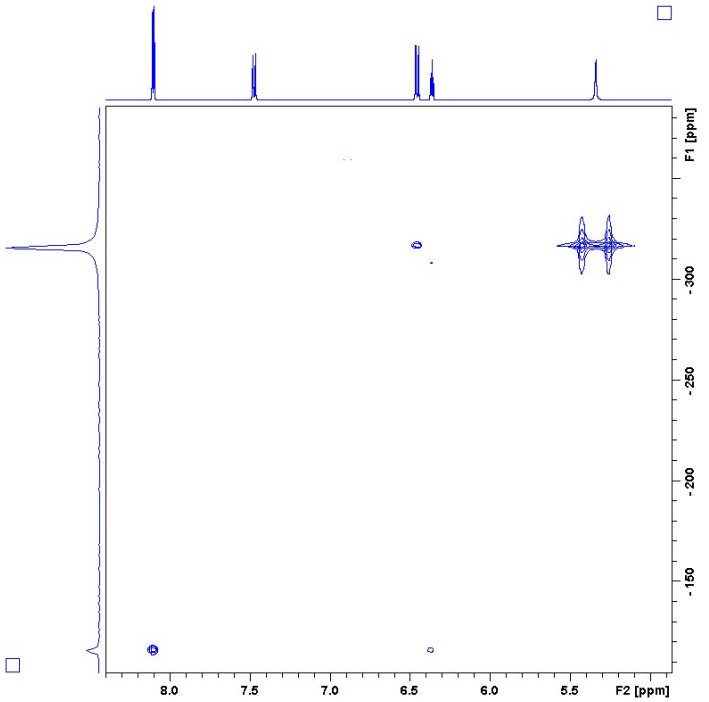

c)

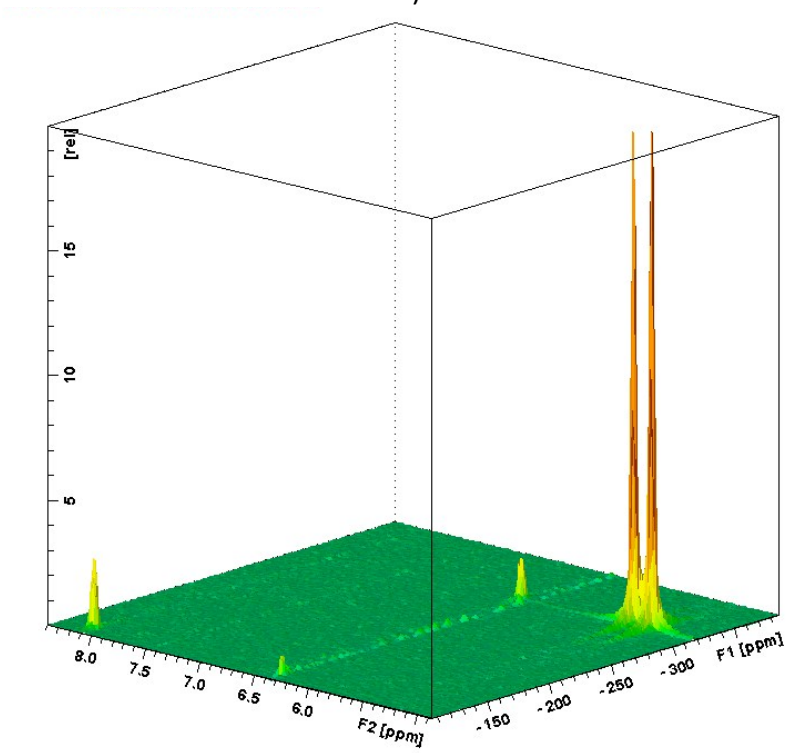

d)

Figure S4 NMR analysis of Na$\mathbf{L}^{\mathbf{SZ}}$ in CD_3SOCD_3, a) ^{1}H, b) ^{13}C, c) contour [^{1}H–^{15}N] HMBC and d) oblique [^{1}H–^{15}N] HMBC spectra.

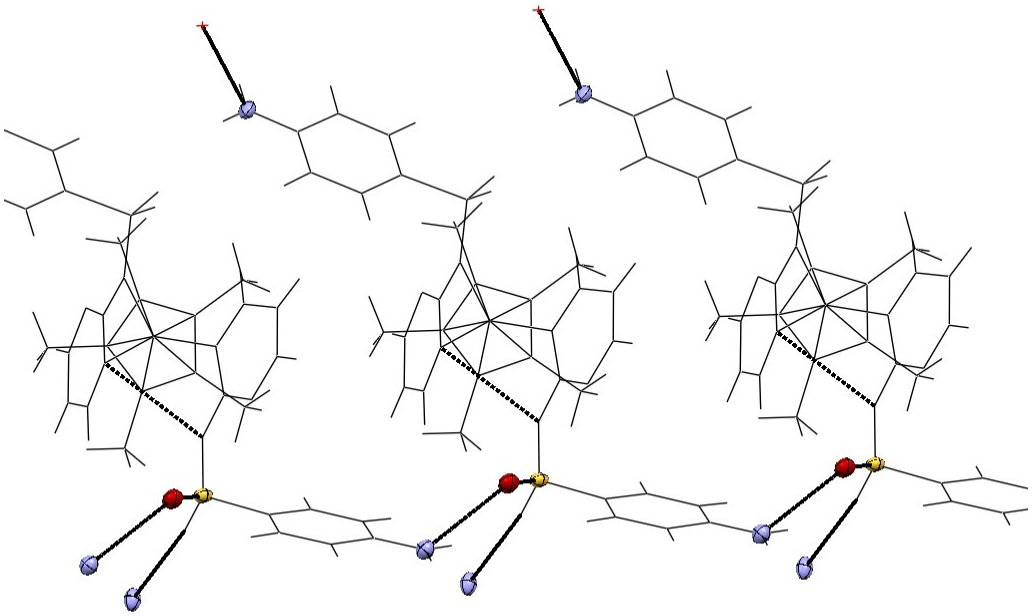

Figure S5 Crystal packing of **2** showing the intermolecular H-bond of the type NH_2…OSO_2.

Table S1 Selected bond lengths and angles of organometal compounds **1** and **2**.*		
1	**2**	
	Calculated	Crystal data
Ru–C2 = 2.295	Rh–C2 = 2.212	Rh–C1_1 = 2.167(2)
Ru–C3 = 2.234	Rh–C3 = 2.208	Rh–C2_1 = 2.147(2)
Ru–C5 = 2.253	Rh–C4 = 2.219	Rh–C3_1 = 2.140(2)
Ru–C7 = 2.297	Rh–C5 = 2.216	Rh–C4_1 = 2.140(2)
Ru–C8 = 2.265	Rh–C6 = 2.178	Rh–C5_1 = 2.132(2)
Ru–C10 = 2.224	Rh–N27 = 2.133	Rh–N1_2 = 2.117(2)
Ru–N26 = 2.147	Rh–N53 = 2.145	Rh–N1_5 = 2.137(2)
Ru–N35 = 2.145	Rh–N62 = 2.172	Rh–N1_6 = 2.172(2)
Ru–N52 = 2.168		
N26–Ru–N35 = 61.1	N27–Rh–N62 = 89.8	N1_2–Rh–N1_5 = 82.93(7)
N52–Ru–N61 = 46.2	N53–Rh–N62 = 61.3	N1_2–Rh–N1_6 = 83.75(7)
N26–Ru–N52 = 84.3	N27–Rh–N53 = 86.3	N1_5–Rh–N1_6 = 61.12(7)
N35–Ru–N61 = 71.1	N36–Rh–N53 = 69.6	

*Numbering of atoms is according to the structures given below. Ground-state geometry optimization of **1** and **2** were carried at B3LYP/Genecp (LANL2DZ for Ru, SDD for Rh, and 6-31G(d) for the rest of the elements) level of theory

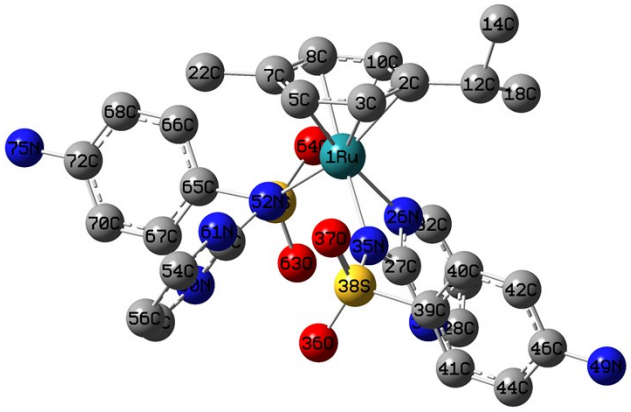

1

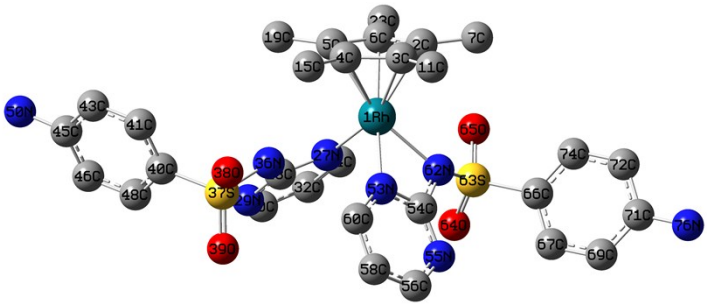

2

Table S2 Computed excitation energies (eV), electronic transition configurations and oscillator strengths (*f*) of the studied complexes (selected, (*f* > 0.002) calculated at CAM-B3LYP/LANL2DZ level of theory.			
Energy (cm^{-1})	Wavelength (nm)	*f*	Major contributions
• **1**			
20618	485	0.0014	HOMO→LUMO+2 (21%)
21959	455	0.0021	HOMO–4→LUMO+2 (14%)
22134	451	0.0035	HOMO–4→LUMO+1 (16%), HOMO–2→LUMO+1 (22%), HOMO→LUMO+1 (26%)
23053	433	0.0009	HOMO–7→LUMO+1 (10%), HOMO–7→LUMO+2 (19%), HOMO–4→LUMO+2 (17%)
26173	382	0.0005	HOMO–2→L+2 (16%), HOMO→LUMO+1 (11%)
28376	352	0.0165	HOMO–7→LUMO+1 (16%), HOMO–4→LUMO+1 (30%)
34291	291	0.035	HOMO→LUMO (43%), HOMO→LUMO+2 (11%)
39244	254	0.1173	HOMO–10→LUMO (11%), HOMO–6→LUMO (11%), HOMO–4→LUMO (20%)
42578	232	0.2492	HOMO–3→LUMO (15%)
• **2**			
21994	454	0.0083	HOMO–3→LUMO (47%)
23282	429	0.0145	HOMO–4→LUMO (40%)
26082	383	0.0159	HOMO–3→LUMO+1 (22%)
26408	378	0.014	HOMO–4→LUMO+1 (34%)
35134	284	0.129	HOMO–2→LUMO+3 (34%), HOMO→LUMO+3 (40%)
43135	231	0.1196	HOMO–3→LUMO+3 (42%)

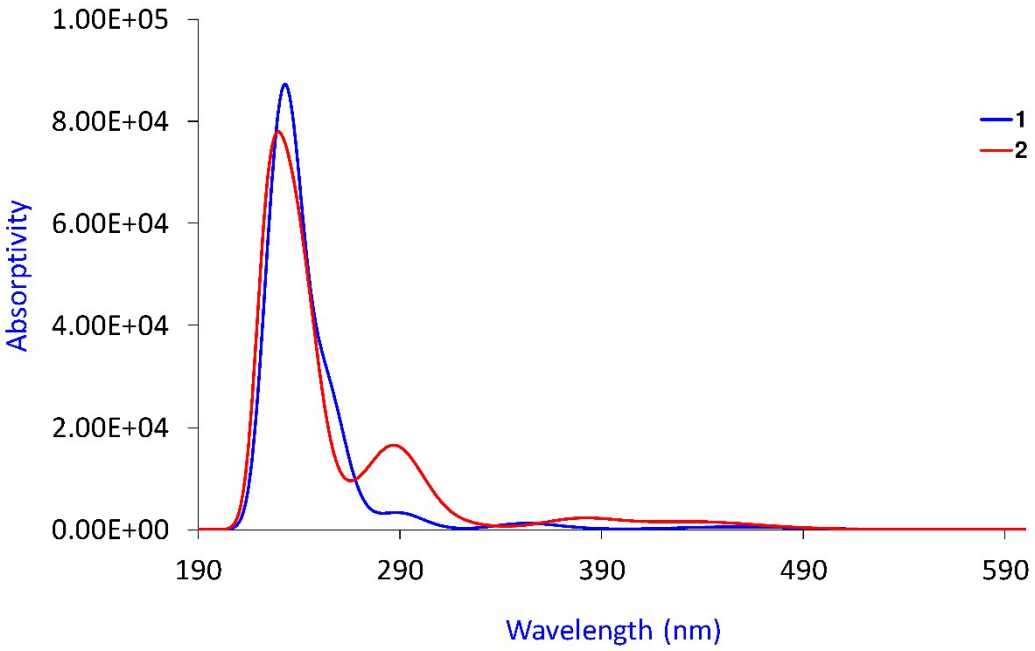

a)

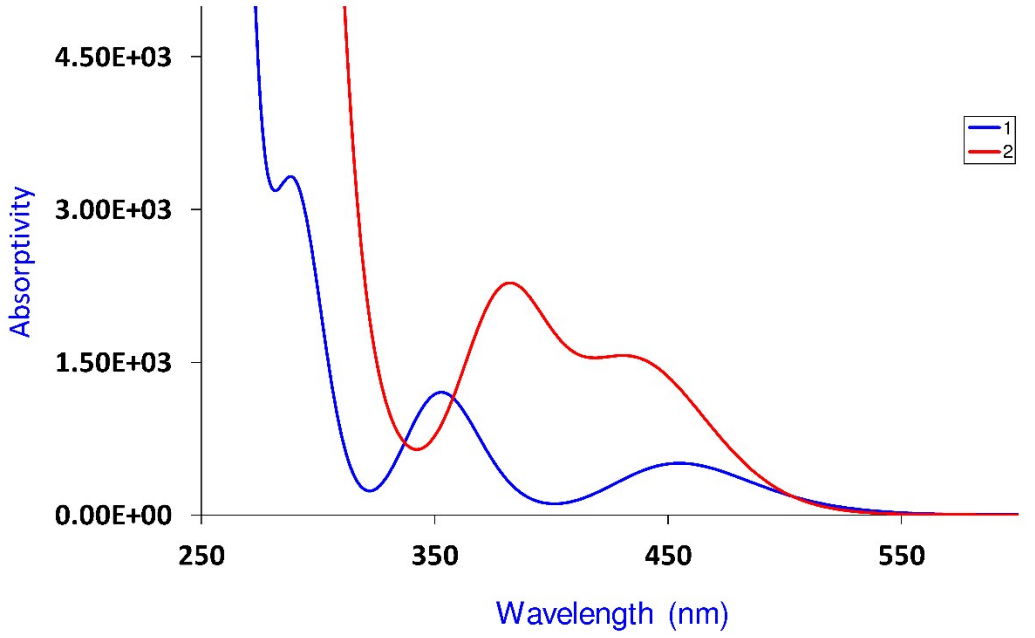

b)

Figure S6 Calculated electronic spectra of the complexes studied here using CAM-B3LYP/LANL2DZ method; a) full spectrum and b) 250–600 nm.

Biological activity testing

Evaluation of antimicrobial properties

The antimicrobial activities of the ligand and its complexes were evaluated against cultures of *Staphylococcus aureus* ATCC 43300, *Escherichia coli* ATCC 25922, *Klebsiella pneumoniae* ATCC 700603, *Acinetobacter baumannii* ATCC 19606, *Pseudomonas aeruginosa* ATCC 27853, as well as two fungi, *Candida albicans* ATCC 90028 and *Cryptococcus neoformans var. grubii* H99; ATCC 208821. The samples were prepared in DMSO to a final testing concentration of 32 µg/mL and serially diluted 1:2 fold for 8 times. Each concentration was prepared in 384-well plates, non-binding surface plate (NBS; Corning 3640) for each bacterial/fungal strain, all in duplicate (n=2), and keeping the final DMSO concentration to a maximum of 0.5%. All bacteria were cultured in Cation-adjusted Mueller Hinton broth at 37 °C overnight. A sample of each culture was then diluted 40-fold in fresh broth and incubated at 37 °C for 1.5-3 h. The resultant mid-log phase cultures were diluted (CFU/mL, measured the absorbance at 600 nm), then added to each well of the compound containing plates, giving a cell density of 5×10^5 CFU/mL and a total volume of 50 µL. All the plates were covered and incubated at 37 °C for 18 h without shaking. The inhibition of the bacterial growth was determined by OD_{600} using a Tecan M1000 Pro monochromator plate reader. The percentage of growth inhibition was calculated for each well, using the negative control (media only) and positive control (bacteria without inhibitors) on the same plate as references. The MIC was determined as the lowest concentration at which the growth was fully inhibited, defined by an inhibition ≥ 80%. In addition, the maximal percentage of growth inhibition is reported as D_{Max}, indicating any compounds with partial activity plates.

Fungi strains were cultured for 3 days on Yeast Extract-peptone Dextrose agar at 30 °C. A yeast suspension of 1×10^6 to 5×10^6 CFU/mL (determined by OD_{600}) was prepared from five colonies. The suspension was subsequently diluted and added to each well of the sample-containing plates giving a cell density of fungi suspension of 2.5×10^3 CFU/mL and total volume of 50 µL. All plates were covered and incubated at 35 °C for 36 h without shaking. The growth inhibition of *Candida albicans* was measured at 630 nm, while that of *Cryptococcus neoformans* was determined by measuring the difference in absorbance at 600 and 570 nm, after the addition of resazurin (0.001%, final concentration) and incubation at 35 °C for 2 h. The absorbance was measured using a Biotek Multiflo Synergy HTX plate reader and controls. The MIC was determined as the lowest concentration at which the growth was fully inhibited, defined by an inhibition = 80% for *Candida albicans* and an inhibition = 70% for *Cryptococcus neoformans*. Due to a higher variance in the growth and inhibition, a lower

threshold was applied to the data for *Cryptococcus neoformans*. In addition, the maximal percentage of growth inhibition is reported as D_{Max}, indicating any compounds with marginal activity.

Cytotoxicity Assay

Human embryonic kidney HEK293 cells were counted manually in a Neubauer haemocytometer and then plated in the 384-well plates containing the compounds to give a density of 5000 cells/well in a final volume of 50 µL. Dulbecco's Modified Eagle Medium (DMEM) supplemented with 10% FBS was used as growth media and the cells were incubated together with the compounds for 20 h at 37 °C in 5% CO_2. Cytotoxicity (or cell viability) was measured by Fluorescence (excitation 560/10, emission 590/10 nm) ($F_{560/590}$), after addition of 5 µL of 25 µg/mL resazurin (2.3 µg/mL final concentration) and after incubation for further 3 h at 37 37 °C in 5% CO_2. The intensity was measured using Tecan M1000 Pro monochromator plate reader, using automatic gain calculation. CC_{50} (the concentration at 50% cytotoxicity) was calculated by curve fitting the inhibition values *vs.* logC using a sigmoidal dose-response function, with variable fitting values for bottom, top and slope. The curve fitting was implemented using Pipeline Pilot's dose-response component, resulting in similar values to curve fitting tools such as GraphPad's Prism and IDBS's XlFit.